

# Scattered Ly $\alpha$ Radiation Around Sources Before Cosmological Reionization

Abraham Loeb and George B. Rybicki

Harvard-Smithsonian Center for Astrophysics, 60 Garden Street, Cambridge, MA 02138

## ABSTRACT

The spectra of the first galaxies and quasars in the Universe should be strongly absorbed shortward of their rest-frame Ly $\alpha$  wavelength by neutral hydrogen (HI) in the intervening intergalactic medium. However, the Ly $\alpha$  line photons emitted by these sources are not eliminated but rather scatter until they redshift out of resonance and escape due to the Hubble expansion of the surrounding intergalactic HI. We calculate the resulting brightness distribution and the spectral shape of the diffuse Ly $\alpha$  line emission around high redshift sources, before the intergalactic medium was reionized. Typically, the Ly $\alpha$  photons emitted by a source at  $z_s \sim 10$  scatter over a characteristic angular radius of  $\sim 15''$  around the source and compose a line which is broadened and redshifted by  $\sim 10^3 \text{ km s}^{-1}$  relative to the source. The scattered photons are highly polarized. Detection of the diffuse Ly $\alpha$  halos around high redshift sources would provide a unique tool for probing the neutral intergalactic medium before the epoch of reionization. On sufficiently large scales where the Hubble flow is smooth and the gas is neutral, the Ly $\alpha$  brightness distribution can be used to determine the cosmological mass densities of baryons and matter.

*Subject headings:* cosmology: theory – line: profiles

## 1. Introduction

Following cosmological recombination at  $z \approx 10^3$ , the Universe became predominantly neutral and hence optically-thick to Ly $\alpha$  photons. The first galaxies that lit up at lower redshifts were surrounded by a neutral intergalactic medium. Their observed spectrum should therefore show a deep trough shortward of their rest-frame Ly $\alpha$  wavelength due to absorption by neutral hydrogen (HI) along the line-of-sight, the so-called Gunn-Peterson effect (Gunn & Peterson 1965). For typical cosmological parameters, the optical depth at the Ly $\alpha$  resonance is so large that one might naively expect the damping wing of the Ly $\alpha$  trough to eliminate any trace of a Ly $\alpha$  emission line in the observed source spectrum (Miralda-Escudé & Rees 1998; Miralda-Escudé 1998). However, here we point out that the Ly $\alpha$  line photons absorbed by intergalactic HI are subsequently re-emitted and hence do not get destroyed<sup>1</sup>. Rather, these photons scatter and diffuse in frequency to the red

---

<sup>1</sup>At the redshifts of interest,  $z_s \sim 10$ , the low densities and lack of chemical enrichment of the IGM make the destruction of Ly $\alpha$  photons by two-photon decay or dust absorption unimportant.

of the Ly $\alpha$  resonance due to the Hubble expansion of the surrounding HI. Eventually, when their net frequency redshift is sufficiently large, they escape and travel freely towards the observer. In this paper we calculate the resulting brightness distribution and spectral line profile of the diffuse Ly $\alpha$  radiation around high-redshift sources<sup>2</sup>.

The lack of a Gunn-Peterson trough (i.e., the detection of transmitted flux shortward of the Ly $\alpha$  wavelength at the source redshift) in the observed spectra of galaxies at  $z \lesssim 5.6$  (Dey et al. 1998; Hu, Cowie, & McMahon 1998; Spinrad et al. 1998; Weymann et al. 1998) implies that most of the intergalactic hydrogen in the Universe was reionized before then. Indeed, popular cosmological models predict that reionization took place around a redshift  $z \sim 10$  (e.g., Haiman & Loeb 1998a,b; Gnedin & Ostriker 1997). At earlier times, the abundance of ionizing sources was small and each of these sources produced an expanding HII region in the surrounding intergalactic medium (IGM). The volume filling factor of HII increased dramatically as the number of ionizing sources grew and their associated HII regions expanded. Eventually, these HII regions overlapped and hydrogen throughout most of the cosmic volume became ionized<sup>3</sup> (Loeb 1997). Subsequently, the ionizing background radiation penetrated the denser HI condensations around collapsed objects (Miralda-Escudé et al. 1998; Barkana & Loeb 1999).

The physics of reionization involves complicated gas dynamics and radiative transfer. Numerical simulations had only recently started to incorporate the relevant equations of radiative transfer rigorously (Abel, Norman, & Madau 1998). The detection of diffuse Ly $\alpha$  photons around high-redshift sources offers an important empirical tool for probing the neutral IGM before and during the reionization epoch, and can be used to test related theoretical calculations. In this context, one is using the Ly $\alpha$  source as a light bulb which illuminates the HI fog in the surrounding IGM. Fortunately, the highest redshift galaxies are found to be strong Ly $\alpha$  emitters (see, e.g. Dey et al. 1998), probably due to their low dust content.

In this paper we calculate the intensity distribution of the diffuse Ly $\alpha$  line in the simplest setting of a pure Hubble flow in a neutral IGM around a steady point source. We leave more complicated configurations for future work. In §2 we describe the formalism and derive analytical solutions in the diffusion regime. In §3 we present a complete numerical solution to this problem using a Monte-Carlo simulation. The detectability of Ly $\alpha$  halos is discussed in §4. Finally, §5 summarizes the implications of our results.

---

<sup>2</sup>The photons absorbed in the Gunn-Peterson trough are also re-emitted by the IGM around the source. However, since these photons originate on the blue side of the Ly $\alpha$  resonance, they travel a longer distance from the source than the Ly $\alpha$  line photons do, before they escape to the observer. The Gunn-Peterson photons are therefore scattered from a larger and hence dimmer halo around the source. The Gunn-Peterson halo is made even dimmer relative to the Ly $\alpha$  line halo, by the fact that the luminosity of the source per unit frequency is often much lower in the continuum than in the Ly $\alpha$  line. We therefore focus on the Ly $\alpha$  line halo in this paper.

<sup>3</sup>Note, however, that even after much of the IGM was ionized, the optical depth at the Ly $\alpha$  resonance was still substantial due to the small residual abundance of HI. Estimates indicate that the reionized Universe provided a measurable transmission of Ly $\alpha$  photons only around  $z \lesssim 7$  (Haiman & Loeb 1998; Miralda-Escudé et al. 1998).

## 2. Analytical Formalism

Although the radiative transfer of line radiation was treated in the past for different geometries of stationary (Harrington 1973) or moving (Neufeld & McKee 1988) atmospheres, no particular attention was given to the cosmological context. As a first treatment of this involved problem, we consider here the transfer of the Ly $\alpha$  line in a uniform, fully neutral IGM, which follows a pure Hubble expansion around a steady point source. As shown later, the diffuse Ly $\alpha$  emission around a high-redshift source could extend over sufficiently large radii where these idealized assumptions are indeed valid.

For newly created Ly $\alpha$  photons the IGM is very opaque, and during scattering events the photon frequencies are redistributed *symmetrically* away from the line center due to the isotropic distribution of thermal velocities of the hydrogen atoms. However, as the photon frequencies drift away from resonance and the medium becomes less opaque, the *asymmetric* redshift bias imposed by the Hubble expansion of the surrounding IGM becomes dominant. Since the IGM is still highly opaque when the redshift effect starts to dominate<sup>4</sup>, we focus in the following only on the Hubble expansion when calculating the *observed* intensity distribution around the source. In terms of the comoving frequencies used here, this implies that the scattering may be regarded as coherent (elastic).

We consider a source surrounded by a spherically-symmetric atmosphere of neutral hydrogen with a linear radial velocity:  $v(r) = H_s r$ , where  $H_s$  is the Hubble expansion rate at the source redshift,  $z_s$ . Let  $I = I(\nu, \mu, r)$  be the specific intensity (in photons  $\text{cm}^{-2} \text{s}^{-1} \text{sr}^{-1} \text{Hz}^{-1}$ ) at comoving frequency  $\nu$  in a direction  $\mu = \cos \theta$  relative to the radius vector at radius  $r$ , as seen by an observer comoving with the gas (i.e. in the cosmic rest frame). Assuming isotropic coherent scattering, the comoving transfer equation for a line at a resonant frequency  $\nu_0$  is then given by,

$$\mu \frac{\partial I}{\partial r} + \frac{(1 - \mu^2)}{r} \frac{\partial I}{\partial \mu} + \alpha \frac{\partial I}{\partial \nu} = \chi_\nu (J - I) + S, \quad (1)$$

where  $\nu$  is the frequency redshift, namely the resonant frequency  $\nu_0$  minus the photon frequency;  $\chi_\nu$  is the scattering opacity at  $\nu$ ;  $J = \frac{1}{2} \int_{-1}^1 d\mu I$  is the mean intensity;  $S$  is the emission function for newly created photons (in photons  $\text{cm}^{-3} \text{s}^{-1} \text{sr}^{-1} \text{Hz}^{-1}$ ); and

$$\alpha \equiv \frac{H_s \nu_0}{c} = 2.7 \times 10^{-13} h_0 \left[ \Omega_M (1 + z_s)^3 + (1 - \Omega_M - \Omega_\Lambda) (1 + z_s)^2 + \Omega_\Lambda \right]^{1/2} \text{Hz cm}^{-1}, \quad (2)$$

with  $\Omega_M$  and  $\Omega_\Lambda$  being the density parameters of matter and the cosmological constant, and  $h_0$  being the current Hubble constant,  $H_0$ , in units of  $100 \text{ km s}^{-1} \text{Mpc}^{-1}$ . Note that at sufficiently high redshifts the value of  $\alpha$  does not depend on  $\Omega_\Lambda$ . The source function on the right-hand-side

---

<sup>4</sup>The neutral IGM is even colder than the microwave background prior to reionization. The corresponding thermal velocities of hydrogen atoms at  $z \lesssim 30$  are smaller by  $\gtrsim 3$  orders of magnitude than the Doppler velocity shift required for the cosmological escape of resonant Ly $\alpha$  photons ( $\sim 10^3 \text{ km s}^{-1}$ ).

of equation (1) can be written as

$$S = \frac{\dot{N}_\alpha}{(4\pi)^2 r^2} \delta(\nu) \delta(r), \quad (3)$$

where  $\dot{N}_\alpha = \text{const}$  is the steady emission rate of Ly $\alpha$  photons by the source (in photons s<sup>-1</sup>).

In terms of our frequency variable, the Ly $\alpha$  opacity is given by (Peebles 1993, p. 573),

$$\chi_\nu = \left(1 - \frac{\nu}{\nu_0}\right)^4 \frac{\beta}{\nu^2 + \Lambda^2 [1 - \nu/\nu_0]^6 / 16\pi^2}, \quad (4)$$

where  $\nu_0 = 2.47 \times 10^{15}$  Hz is the Ly $\alpha$  frequency,  $\Lambda = 6.25 \times 10^8$  s<sup>-1</sup> is the rate of spontaneous decay from the 2p to the 1s energy levels of hydrogen, and

$$\beta \equiv \left(\frac{3c^2 \Lambda^2}{32\pi^3 \nu_0^2}\right) n_{\text{HI}} = 1.5 \Omega_b h_0^2 (1 + z_s)^3 \text{ cm}^{-1} \text{ Hz}^2. \quad (5)$$

Here  $n_{\text{HI}}$  is the mean hydrogen density in the (neutral) IGM at a redshift  $z_s$ , expressed in terms of the current baryonic density parameter,  $\Omega_b$ , and the normalized Hubble constant,  $h_0$ . For typical cosmological parameters, the mean-free-path at the line center is negligible compared to the size of the system. Hence, a distant observer would see only those photons which scatter to the wings of the line, where to a good approximation the opacity scales as,

$$\chi_\nu \approx \frac{\beta}{\nu^2}, \quad (6)$$

with  $\beta$  being a constant due to the assumed uniformity of the IGM. This approximate relation holds as long as the frequency shift is small,  $\nu/\nu_0 \ll 1$ , and is adequate throughout the discussion that follows.

Before proceeding, we should point out that the transfer problem described by equation (1) is completely analogous to that of time-dependent monochromatic isotropic scattering, where the frequency  $\nu$  here plays the role of “time.” This is easily understood, since a photon is subjected to a constant redshifting due to the Hubble expansion, and the scattering is coherent, so its frequency is a perfect surrogate for time. This implies that the problem can be viewed as an initial value problem in frequency, so the solution for a fixed frequency determines the behavior of the solution at all other frequencies. One should note, however, when using this analogy that the opacity law here is a decreasing function of “time.”

We would now like to normalize the frequency shift and radius in the problem by convenient scales. An appropriate frequency scale,  $\nu_\star$ , is introduced by equating the Ly $\alpha$  optical depth from the source to the observer to unity,

$$\tau_\nu = \int_0^\infty \frac{\beta}{(\nu_\star + \alpha r)^2} dr = \frac{\beta}{\alpha \nu_\star} = 1, \quad (7)$$

yielding

$$\nu_\star = \frac{\beta}{\alpha} = 5.6 \times 10^{12} \Omega_b h_0 \left[ \Omega_M (1 + z_s)^{-3} + (1 - \Omega_M - \Omega_\Lambda) (1 + z_s)^{-4} + \Omega_\Lambda (1 + z_s)^{-6} \right]^{-1/2} \text{ Hz}. \quad (8)$$

Note that for the popular values of  $\Omega_b \approx 0.05$ ,  $\Omega_M = 0.4$ ,  $\Omega_\Lambda = 0.6$  and  $h_0 = 0.65$  (e.g., Turner 1999, and references therein), the frequency shift of the photons which escape to infinity is  $(\nu_\star/\nu_0) \approx 4 \times 10^{-3}$  at  $z_s = 10$ . This corresponds to a spectroscopic velocity shift of  $(\nu_\star/\nu_0)c \sim 10^3 \text{ km s}^{-1}$  at the source. The proper radius where the Doppler shift due to the Hubble expansion produces the above frequency shift is given by  $r_\star = \nu_\star/\alpha$ , or

$$r_\star = \frac{\beta}{\alpha^2} = \frac{2.1 \times 10^{25} (\Omega_b/\Omega_M) \text{ cm}}{\left[1 + (1 - \Omega_M - \Omega_\Lambda)\Omega_M^{-1}(1 + z_s)^{-1} + (\Omega_\Lambda/\Omega_M)(1 + z_s)^{-3}\right]} \approx 6.7 \left(\frac{\Omega_b}{\Omega_M}\right) \text{ Mpc}, \quad (9)$$

The last equality was obtained for high redshifts,  $z_s \gg 1$ . We thus find that for an  $\Omega_M = 1$ ,  $\Omega_\Lambda = 0$  cosmology or at high redshifts for any other cosmology, the physical distance  $r_\star$  is independent of the source redshift and depends only on the baryonic mass fraction,  $F_b \equiv \Omega_b/\Omega_M$ . This fraction can be calibrated empirically from X-ray data on clusters of galaxies (Carlberg et al. 1998; Ettori & Fabian 1999) which yield a value of  $F_b \approx 0.1$  for  $h_0 = 0.65$ . Note that  $\nu_\star$  was derived at the source rest frame; its value is lower by a factor of  $(1 + z_s)$  in the observer's frame.

It is convenient for further developments to rescale the variables in the problem and make them dimensionless. Radius and frequency are rescaled using the characteristic quantities  $r_\star$  and  $\nu_\star$ , that is,  $\tilde{r} \equiv (r/r_\star)$  and  $\tilde{\nu} \equiv (\nu/\nu_\star)$ . We rescale all radiation quantities using the characteristic quantity  $I_\star = \dot{N}_\alpha/(r_\star^2 \nu_\star)$ , that is,  $\tilde{I} = I/I_\star$ ,  $\tilde{J} = J/I_\star$ , etc. We also define the rescaled source term,

$$\tilde{S} = \frac{S r_\star}{I_\star} = \frac{1}{(4\pi)^2 \tilde{r}^2} \delta(\tilde{\nu}) \delta(\tilde{r}) \quad (10)$$

Equation (1) can then be written in dimensionless coordinates,

$$\mu \frac{\partial \tilde{I}}{\partial \tilde{r}} + \frac{(1 - \mu^2)}{\tilde{r}} \frac{\partial \tilde{I}}{\partial \mu} + \frac{\partial \tilde{I}}{\partial \tilde{\nu}} = \frac{1}{\tilde{\nu}^2} (\tilde{J} - \tilde{I}) + \tilde{S}, \quad (11)$$

Next, we take the first two angular moments of equation (11). In addition to  $\tilde{J}$ , these will involve the two moments  $\tilde{K} = \frac{1}{2} \int_{-1}^1 d\mu \mu^2 \tilde{I}$ , and  $\tilde{H} = \frac{1}{2} \int_{-1}^1 d\mu \mu \tilde{I}$ . In order to close the above system of equations, one needs a relation between  $\tilde{J}$  and  $\tilde{K}$ . The closure relation is often parameterized through the Eddington factor  $f = f(\nu, r) \equiv \tilde{K}/\tilde{J}$  (Hummer & Rybicki 1971; Mihalas 1978). This parametrization yield for the comoving transfer equation (Mihalas, Kunasz, & Hummer 1976),

$$\frac{1}{\tilde{r}^2} \frac{\partial(\tilde{r}^2 \tilde{H})}{\partial \tilde{r}} + \frac{\partial \tilde{J}}{\partial \tilde{\nu}} = \tilde{S} \quad (12)$$

and

$$\frac{\partial(f \tilde{J})}{\partial \tilde{r}} + \frac{(3f - 1)}{\tilde{r}} \tilde{J} + \frac{\partial \tilde{H}}{\partial \tilde{\nu}} = -\frac{\tilde{H}}{\tilde{\nu}^2}. \quad (13)$$

## 2.1. The Extended Eddington Approximation

We can close the above set of equations by specifying the radial and frequency dependence of the Eddington factor  $f$ . The simplest choice is to use the Eddington approximation  $f = 1/3$ , which is expected to be valid at large optical depths in the medium. However, for the moment we assume  $f$  to be a constant, but not necessarily equal to  $1/3$ .

For convenience, we define the rescaled variables  $h \equiv \tilde{r}^2 \tilde{H}$ ,  $j \equiv \tilde{r}^2 \tilde{J}$ , and  $s = \tilde{r}^2 \tilde{S}$ . This yields,

$$\frac{\partial h}{\partial \tilde{r}} = -\frac{\partial j}{\partial \tilde{\nu}} + s, \quad (14)$$

and

$$f \frac{\partial j}{\partial \tilde{r}} - (1-f) \frac{j}{\tilde{r}} = -\frac{\partial h}{\partial \tilde{\nu}} - \frac{h}{\tilde{\nu}^2}. \quad (15)$$

By taking the  $\tilde{r}$ -derivative of equation (15) and substituting the  $\tilde{\nu}$ -derivative of equation (14) into it, we get

$$\frac{\partial}{\partial \tilde{r}} \left( f \frac{\partial j}{\partial \tilde{r}} - [1-f] \frac{j}{\tilde{r}} \right) = \frac{\partial^2 j}{\partial \tilde{\nu}^2} + \frac{1}{\tilde{\nu}^2} \frac{\partial j}{\partial \tilde{\nu}} - \frac{\partial s}{\partial \tilde{\nu}} - \frac{s}{\tilde{\nu}^2}. \quad (16)$$

If we now define the function

$$g = f \tilde{r}^{-[1-f]/f} j \equiv f \tilde{r}^{[3f-1]/f} \tilde{J}. \quad (17)$$

then equation (16) can be written as,

$$\frac{\partial g}{\partial \tilde{\nu}} - f \tilde{\nu}^2 \left( \frac{1}{\tilde{r}^{[1-f]/f}} \frac{\partial}{\partial \tilde{r}} \tilde{r}^{[1-f]/f} \frac{\partial g}{\partial \tilde{r}} - \frac{1}{f} \frac{\partial^2 g}{\partial \tilde{\nu}^2} \right) = \tilde{\nu}^2 \frac{\partial \tilde{s}}{\partial \tilde{\nu}} + \tilde{s}, \quad (18)$$

where  $\tilde{s} = f \tilde{r}^{[3f-1]/f} \tilde{S}$ .

Equation (18) resembles the *causal* diffusion equation (Narayan, Loeb, & Kumar 1994, and references therein), with the substitution of frequency shift for time, and a “diffusion” coefficient  $D = f \tilde{\nu}^2$ . The Ly $\alpha$  photons are expected to redshift away from the line center at a rate which is dictated by this diffusion coefficient. Inspection of the second-order terms provides the condition for “causality” in this problem, namely  $\tilde{\nu} \geq \tilde{r}/\sqrt{f}$ . This condition has a simple interpretation: the frequency shift at any given radius is greater than the Doppler shift due to the Hubble velocity there, since the photon could have scattered multiple times before arriving at that radius. Unfortunately, the line opacity is not constant and the above diffusion equation is complicated by the frequency dependence of the diffusion coefficient.

Equation (18) requires a particular choice for the value of  $f$ . There are two physical regimes where the assumption of  $f = \text{const}$  holds: (i) the diffusion regime where the optical depth is high and  $f \approx 1/3$ , and (ii) the free-streaming regime where the optical depth is low and  $f \approx 1$ . Note that  $g = \frac{1}{3} \tilde{J}$  in the first regime and  $g = \tilde{r}^2 \tilde{J}$  in the second. In the diffusion regime, the number of scatterings is large and so  $\nu \gg \alpha r$  or  $\tilde{\nu} \gg \tilde{r}$ . This implies that the  $\partial_{\tilde{\nu}}^2 g$  term can be neglected relative to the  $\nabla_{\tilde{r}}^2 g$  term in equation (18) and the problem is simplified considerably. Such a simplification is not possible in the free-streaming case. We therefore focus next on the diffusion regime where  $\tilde{r} \ll \tilde{\nu} \ll 1$ , and  $f \approx 1/3$ .

## 2.2. The Diffusion Solution

In the diffusion regime, equation (18) reads

$$\frac{\partial \tilde{J}}{\partial \tilde{\nu}} - \frac{\tilde{\nu}^2}{3} \frac{1}{\tilde{r}^2} \frac{\partial}{\partial \tilde{r}} \tilde{r}^2 \frac{\partial \tilde{J}}{\partial \tilde{r}} = \delta(\tilde{\nu}) \frac{\delta(\tilde{r})}{(4\pi)^2 \tilde{r}^2}. \quad (19)$$

With the definition of a new variable,  $\sigma = (\tilde{\nu}^3/9)$ , we get the standard diffusion equation in spherical geometry,

$$\frac{\partial \tilde{J}}{\partial \sigma} - \nabla^2 \tilde{J} = \frac{1}{4\pi} \delta(\sigma) \delta(\tilde{\mathbf{r}}), \quad (20)$$

where  $\mathbf{r}$  is the radius vector, and where  $\sigma$  now plays the role of the usual time variable. The solution to this equation for  $\nu > 0$  (redshifted photons) is

$$\tilde{J} = \frac{1}{(4\pi)^{5/2} \sigma^{3/2}} e^{-\tilde{r}^2/4\sigma} = \frac{1}{4\pi} \left( \frac{9}{4\pi \tilde{\nu}^3} \right)^{3/2} \exp \left\{ -\frac{9\tilde{r}^2}{4\tilde{\nu}^3} \right\}. \quad (21)$$

This solution satisfies the integral relation,

$$(4\pi)^2 \int_0^\infty \tilde{J} \tilde{r}^2 d\tilde{r} = 1, \quad (22)$$

which follows by performing the Gaussian integral, or directly from the diffusion equation (19). In a way this may be viewed as a result of photon conservation, since frequency here is analogous to time in the usual diffusion equation.

Eventually the diffusion solution becomes invalid when the opacity is small enough to allow photons to escape to the observer. Most of the Ly $\alpha$  photons escape to infinity from a smaller radius than  $r_\star$  as they scatter many times and hence redshift in frequency more than  $\alpha r$  at any given radius  $r$ . Even though  $\nu_\star$  and  $r_\star$  may not represent the true parameters of the escaping photons, equations (8) and (9) provide the scaling of the exact numerical solution with model parameters, since we have already shown that these constants can be used to normalize the basic transfer equation (1) and bring it to a scale-free form. Next we proceed to derive the full numerical solution for the escaping radiation in the dimensionless variables  $\tilde{\nu}$  and  $\tilde{r}$ .

## 3. Results from a Monte-Carlo Simulation

The lack of an analytical solution applicable to both the diffusion and free-streaming regimes motivated us to find solutions by numerical means. The Monte Carlo method suggested itself by its generality and ease of formulation. The usual disadvantage of this method of having to treat large numbers of photons is largely irrelevant in the present case, because all the physical parameters have been scaled out of the equations, and only one Monte Carlo run is needed to solve the problem completely.

The Monte Carlo method follows the histories of a large number of photons in accordance with the following rules:

**Step 1:** A newly created photon is chosen from the distribution given by the form of the emission function  $S$ . Ideally we would like this to be a photon with  $\tilde{r} = 0$  and  $\tilde{\nu} = 0$ . However, because of the singularity of the opacity, this cannot be done, so in practice we choose our new photons with a small, but nonzero, frequency (e.g.,  $\tilde{\nu} = 10^{-2}$ ) and use the diffusion solution (21) to determine a random starting value of  $\tilde{r}$ .

**Step 2:** Suppose a photon has been scattered (or has been newly created) at a radius  $\tilde{r}$  and with a frequency  $\tilde{\nu}$ . A random direction is then chosen from an isotropic distribution; this is most easily done by taking  $\mu = 2R - 1$  where  $R$  is a random deviate uniform on the interval  $(0, 1)$ .

To choose a step length for the photon flight, we use the fact that the optical depth  $\tau$  along the ray to the next scattering follows the exponential distribution law,  $\exp(-\tau)$ . This can be simulated by choosing  $\tau = -\ln R'$ , where  $R'$  is another random deviate uniform on the interval  $(0, 1)$ . To convert this to distance, we compute  $\tau$  as,

$$\tau = \int_0^\ell \chi_\nu d\ell' = \int_0^{\tilde{\ell}} \frac{d\tilde{\ell}'}{(\tilde{\nu} + \tilde{\ell}')^2} = \frac{1}{\tilde{\nu}} - \frac{1}{\tilde{\nu} + \tilde{\ell}}, \quad (23)$$

where  $\ell$  is the pathlength along the ray, and  $\tilde{\ell} = \ell/r_\star$ . Taking  $\tilde{\ell} \rightarrow \infty$ , we see that there is a maximum optical depth to infinity,

$$\tau_{\max} = \frac{1}{\tilde{\nu}}. \quad (24)$$

If  $\tau$  is greater than  $\tau_{\max}$ , the photon escapes and we proceed to Step 3. If  $\tau$  is less than  $\tau_{\max}$ , a scattering event will occur. We may then solve equation (23) for the pathlength,

$$\tilde{\ell} = \frac{\tilde{\nu}\tau}{\tau_{\max} - \tau}. \quad (25)$$

At the new scattering site, the photon's new radius  $\tilde{r}'$  and new comoving frequency  $\tilde{\nu}'$  are

$$\tilde{r}' = (\tilde{r}^2 + \tilde{\ell}^2 + 2\tilde{r}\tilde{\ell}\mu)^{1/2}, \quad (26)$$

$$\tilde{\nu}' = \tilde{\nu} + \tilde{\ell}. \quad (27)$$

With the substitutions  $\tilde{r}' \rightarrow \tilde{r}$  and  $\tilde{\nu}' \rightarrow \tilde{\nu}$ , we now repeat Step 2 to find the positions and frequencies of the photon at each of its successive scatterings. This loop is repeated until escape occurs.

**Step 3:** Escape ends the random walk for this photon. We characterize an escaped photon by its scaled impact parameter and its “observed” scaled frequency, relative to the source center,

$$\tilde{p} = \tilde{r}\sqrt{1 - \mu^2}, \quad (28)$$

$$\tilde{\nu}_{\text{obs}} = \tilde{\nu} - \tilde{r}\mu. \quad (29)$$



Here the frequency is still defined at the source rest frame and should be divided by  $(1 + z_s)$  for conversion to the observer’s frame.

Steps 1, 2 and 3 are repeated for as many photons as are necessary to get good statistical estimates for the physical quantities of interest.

In order to relate the results of the Monte Carlo simulations to observable quantities, histograms were constructed. Introducing discrete sets of impact parameters  $\tilde{p}_i$  and “observed” frequencies  $\tilde{\nu}_j$ , the final values for the escaping photons can be binned into a two-dimensional histogram. The “observed” intensity field  $\tilde{I}(\tilde{p}_i, \tilde{\nu}_j)$  is then estimated as proportional to

$$\frac{N_{ij}}{(2\pi\tilde{p}_i\Delta\tilde{p}_i)(\Delta\tilde{\nu}_j)}, \quad (30)$$

where  $N_{ij}$  is the number of photons falling into the  $i, j$  bin of widths  $\Delta\tilde{p}_i$ ,  $\Delta\tilde{\nu}_j$ . Similar estimates can be made for the intensity  $\tilde{I}(\tilde{p})$ , integrated over frequencies, and  $\tilde{I}(\tilde{\nu})$ , integrated over the area of the plane of the sky. Again, we define these intensities at the source frame. For conversion to the observer’s frame,  $\tilde{I}(\tilde{p}_i, \tilde{\nu}_j)$  should be divided by  $(1 + z_s)^2$ , and  $\tilde{I}(\tilde{p})$  should be divided by  $(1 + z_s)^3$  (since the photon phase space density  $I(p, \nu)/\nu^2$  is conserved during the Hubble expansion).

Although the quantities in equations (26) and (27) are not directly observed, it is of theoretical interest to bin them also into a histogram in order to estimate the value of mean intensity at interior points, based on the fact that the number of scatterings per unit volume is proportional to the mean intensity.

A Monte Carlo run using  $10^8$  photons seemed to give satisfactory results for most of the histogram bins. The exceptions are those at small values of the impact parameter or radius, where the corresponding bin areas or volumes become quite small, making the statistical errors large.

The Monte Carlo results are given in Figures 1–5. Figure 1 shows the intensity in the Ly $\alpha$  line integrated over frequency,

$$\tilde{I}(\tilde{p}) = \int_0^\infty \tilde{I}(\tilde{p}, \tilde{\nu}) d\tilde{\nu}, \quad (31)$$

as a function of impact parameter. The intensity has a fairly compact central core; the characteristic impact parameter at which the intensity has fallen to half its central value is only about  $0.1r_\star$ , an order of magnitude less than the characteristic length  $r_\star$ . Because the intensity scales inversely as the square of the characteristic impact parameter, this means that the central intensities are two orders of magnitude larger than a simple estimate might have indicated. The half-light radius  $p_{1/2}$  (i.e., the radius of a circular aperture containing half of the Ly $\alpha$  emission) is further out, at  $0.63r_\star$ , but at that impact parameter the intensity is already down by over an order of magnitude from its central value. Since the sky brightness limits the observational sensitivity, it may be difficult to infer  $p_{1/2}$  observationally. However, since the scattered light is expected to be highly polarized (Rybicki & Loeb 1999), its contrast relative to an unpolarized background could be enhanced by using a polarization filter.

The angular radius on the sky corresponding to the physical radius of  $p = 0.1r_*$  over which the scattered Ly $\alpha$  halo maintains a roughly uniform surface brightness, is given by

$$\theta = \frac{p}{d_A}, \quad (32)$$

where  $d_A$  is the angular diameter distance. In an  $\Omega_\Lambda = 0$  cosmology,  $d_A = 2cH_0^{-1}[\Omega_M z_s + (\Omega_M - 2)(\sqrt{1 + \Omega_M z_s} - 1)]/[\Omega_M^2(1 + z_s)^2]$  (e.g., Padmanabhan 1993), while in an  $\Omega_\Lambda \neq 0$  cosmology the expression is more involved (Edwards 1972, Eisenstein 1997; see also Fig. 13.5 in Peebles 1993). We then find for the example of  $\Omega_M = 0.4$ ,  $\Omega_\Lambda = 0$ ,  $h_0 = 0.65$ , and  $z_s = 10$ , that  $\theta = 15'' \times (p/70 \text{ kpc})$ , with a slightly larger value for a flat  $\Omega_\Lambda = 0.6$  cosmology. Thus, the Ly $\alpha$  luminosity of a typical source at  $z_s \sim 10$  is expected to spread over a characteristic angular radius of  $\sim 15''$  on the sky.

Figure 2 shows the total photon emission rate (luminosity) per unit frequency,

$$\tilde{L}(\tilde{\nu}) = 8\pi^2 \int_0^\infty \tilde{I}(\tilde{p}, \tilde{\nu}) \tilde{p} d\tilde{p}, \quad (33)$$

which can be used to get the observed spectral flux of photons  $F(\nu)$  (in photons  $\text{cm}^{-2} \text{s}^{-1} \text{Hz}^{-1}$ ) from the entire Ly $\alpha$  halo,

$$F(\nu) = \frac{\tilde{L}(\tilde{\nu})}{4\pi d_L^2} \frac{\dot{N}_\alpha}{\nu_*} (1 + z_s)^2, \quad (34)$$

where  $\nu = \tilde{\nu}\nu_*/(1 + z_s)$ , and  $d_L = d_A(1 + z_s)^2$  is the standard luminosity distance to the source. This flux is expressed in the frame of a local observer. The extra factor of  $(1 + z_s)^2$  is due to the fact that we evaluate the photon number flux per unit frequency rather than the energy flux – which is used in the usual definition of  $d_L$ . As mentioned before, the observed intensity is

$$I(p, \nu) = \frac{\tilde{I}(\tilde{p}, \tilde{\nu})}{(1 + z_s)^2} \frac{\dot{N}_\alpha}{r_*^2 \nu_*}, \quad (35)$$

and similarly the observed integral of the intensity over frequency,

$$I(p) = \frac{\tilde{I}(\tilde{p})}{(1 + z_s)^3} \frac{\dot{N}_\alpha}{r_*^2}. \quad (36)$$

The peak of the function  $\tilde{L}(\tilde{\nu})$  is seen to be redshifted by roughly 0.44 (recall that we define  $\tilde{\nu}$  to be the *negative* deviation from line center). The full width at half maximum is  $\Delta\tilde{\nu} = 1.75$ . A linear plot of  $\tilde{L}(\tilde{\nu})$  is presented in Figure 3. Because the shifts are small, the abscissa can be equally interpreted as proportional to wavelength shift from line center, so Figure 3 also shows the observed lineshape as a function of wavelength. One notes the very extended red wing of this line, which goes approximately as  $1/\tilde{\nu}^2$ . Because of this behavior, the centroid of the line is not well defined.

Figure 4 shows the observed intensities as a function of frequency for five different impact parameters ( $\log \tilde{p} = 0.0, -0.5, -1.0, -1.5$ , and  $-2.0$ ). The curves for  $\log \tilde{p} = -1.5$  and  $-2.0$  have

been smoothed, but still show some fluctuations due to limited Monte Carlo sampling, especially at the smallest frequencies. All curves share roughly the same lineshape, and (apart from vertical scaling) differ only in the redshift of the peak. The peak redshift is at a minimum,  $\tilde{\nu} = 0.19$ , for the central rays, and increases to 0.33 for  $\tilde{p} = 0.1$  and to 1.4 for  $\tilde{p} = 1$ . Using appropriate integration, these curves could be used to compute the expected lineshape from observations in specific circular apertures or slits (e.g., Dey et al. 1998).

Figure 5 is mostly of theoretical interest and shows the internal mean intensity as a function of radius for a variety of frequencies. At the smallest frequencies the curves are reasonably well approximated by the diffusion solution (21), shown as the dotted curves. As  $\tilde{\nu}$  increases into the free-streaming regime ( $\tilde{\nu} \gtrsim 1$ ), the curves deviate from the diffusion solution, and eventually become almost shock-like, with photons piling up near the “causality” surface  $\tilde{r} = \tilde{\nu}$ , consistently with the “causal” diffusion equation (18).

One caveat concerning Figure 5 should be noted. Many of these curves exhibited considerable statistical error at small values of  $\tilde{r}$ , especially for the largest values of  $\tilde{\nu}$ . In these uncertain regions the plots were completed by assuming that all curves approach a constant value at small  $\tilde{r}$ , determined by the solution at larger  $\tilde{r}$ . This extrapolation procedure is certainly justified in the diffusion limit, but its validity in the general case needs to be investigated further.

#### 4. Observational Considerations

In this section we consider the detectability of the Ly $\alpha$  halos. Many of the basic properties of the early sources are unknown, and so our estimates are meant for illustrative purposes only.

The cosmological parameters affect our estimates, but not greatly. In this section, we assume  $\Omega_\Lambda = 0$ ,  $\Omega_M = 0.4$ ,  $\Omega_b = 0.05$ , and  $h_0 = 0.65$ . Of greater uncertainty is the Ly $\alpha$  photon luminosity,  $\dot{N}_\alpha$ , of high-redshift sources. For the sake of definiteness, we adopt the measured luminosity for a known Ly $\alpha$  galaxy at  $z_s = 5.34$ , which was discovered by Dey et al. (1998). To estimate the integral under the observed spectral line profile in their Figure 3, we assume an intensity amplitude of  $\sim 5 \mu\text{Jy}$  and a rest-frame line width of  $\sim 2 \text{ \AA}$ . In our cosmological model, this source has a luminosity distance of  $d_L = 1.64 \times 10^{29} \text{ cm}$ , yielding a value of

$$\dot{N}_\alpha = 6.4 \times 10^{53} \text{ s}^{-1}. \quad (37)$$

Let us now assume that a candidate high-redshifted source is identified and its redshift determined by some other unscattered lines, such as H $\alpha$ . As a specific example, suppose the source is at  $z_s = 10$ , so that its observed Ly $\alpha$  line falls in the infrared at  $1.34 \mu\text{m}$ . From equations (8) and (9) we find,

$$\begin{aligned} \nu_\star &= 9.8 \times 10^{12} \text{ Hz}, \\ r_\star &= 2.3 \times 10^{24} \text{ cm} = 745 \text{ kpc}. \end{aligned} \quad (38)$$

The angular diameter distance is found to be  $d_A = 3.0 \times 10^{27}$  cm, implying a typical angular size of the halo of  $0.1 r_*/d_A = 7.7 \times 10^{-5} = 16''$ .

The observed integrated brightness near the center of the halo is given by equation (36). Figure 1 shows that  $\tilde{I}(0) = 0.2$ , and so

$$I_{\text{halo}}(0) = 18 \text{ photons cm}^{-2} \text{ s}^{-1} \text{ sr}^{-1}. \quad (39)$$

We suppose that a narrow filter is used to observe only in a narrow wavelength band containing the Ly $\alpha$  line, in order to reduce the sky background as much as possible. From Figure 3 we infer the Full Width at Half Maximum of the line  $\Delta\tilde{\nu} \approx 1$ , implying an observing filter width of 50 Å for a source at  $z_s = 10$ . However, one could use narrower filters to take advantage of the fact that the monochromatic intensity depends jointly on frequency and impact parameter in a known way, as shown in Figure 4. If one wanted to concentrate only on the innermost core of emission (out to  $\tilde{p} = 0.1$ ), then a width  $\Delta\tilde{\nu} = 0.5$  would be sufficient, implying a filter width of only 25 Å. We adopt this narrower filter width in our estimate of the sky background. In frequency this corresponds to  $\Delta\nu = 4.2 \times 10^{11}$ .

The brightness of the halo is to be compared to the sky background at 1.34  $\mu\text{m}$ , which is obviously minimized in observations from space. Using sufficiently high resolution to eliminate contaminating point sources, the sky brightness from space is dominated by interplanetary dust (IPD) emission. The local IPD contamination might be reduced by having a spacecraft well above the ecliptic plane, but for the moment we shall proceed conservatively and assume that the IPD is the primary sky background. Hauser et al. (1998) quote a value for the IPD brightness at 1.25  $\mu\text{m}$  of  $\sim 375 \text{ nW m}^{-2} \text{ sr}^{-1}$ . This implies a sky brightness within our filter band of

$$I_{\text{sky}} = 4.7 \times 10^5 \text{ photons cm}^{-2} \text{ s}^{-1} \text{ sr}^{-1}. \quad (40)$$

Thus, the halo brightness is only  $\sim 4 \times 10^{-5}$  of the sky background. Given this low value, Ly $\alpha$  halos would be difficult to observe. However, there are a number of reasons for reasonable optimism in the long run for their detection.

The choice of Ly $\alpha$  luminosity in equation (37), based on Dey et al. (1998), was made purely for definiteness. The observed radiation intensity scales linearly with the value of  $\dot{N}_\alpha$ , and so our estimates may be easily modified for any other value. If the values of  $\dot{N}_\alpha$  for some high redshift sources were much larger (e.g. due to higher star formation rates or lower dust content), then the difficulty in observing the Ly $\alpha$  halos would be eased considerably. In this regard we note that even if the value given in equation (37) is typical for high-redshift galaxies, it is likely that there will be a power-law distribution of observed fluxes (see Figure 2 in Haiman & Loeb 1998b), and some sources could have values of  $\dot{N}_\alpha$  larger by factors of ten or more.

In addition, the interplanetary dust emission could be much lower if the orbit of a spacecraft such as the Next Generation Space Telescope (NGST) is chosen so that the telescope spends some of its time outside the orbit of the Earth or well above the ecliptic plane. The limiting noise level

in this case is provided by the cosmic infrared background. This background is poorly known, but Hauser et al. (1998) give an upper limit at  $1.25 \mu\text{m}$  of  $\nu I_0 \sim 75 \text{ nW m}^{-2} \text{ sr}^{-1}$ , a factor of five less than the value adopted in equation (40). Given this sky background, we can calculate the minimum exposure time necessary for the detection of the  $\text{Ly}\alpha$  halo signal. Ignoring instrumental noise and adopting a detector quantum efficiency close to unity (see <http://augusta.stsci.edu/ngst-etc/ngstetc.html>, for more realistic estimates), we can find the best signal-to-noise ratio,  $S/N$ , that is attainable after an exposure time  $t$  on an NGST telescope of 8 meter diameter,

$$\frac{S}{N} = 10 \left( \frac{\dot{N}_\alpha}{6 \times 10^{54} \text{ s}^{-1}} \right) \left( \frac{t}{10 \text{ hours}} \right)^{1/2} \quad (41)$$

Hence, the halo of a source at  $z_s \lesssim 10$  which is an order of magnitude brighter in  $\text{Ly}\alpha$  than the Dey et al. (1998) galaxy might be detectable.

Another circumstance favoring such observations is that the  $\text{Ly}\alpha$  halos are highly polarized (see Rybicki & Loeb 1999). This polarization is highest at the outermost radii, but is  $\sim 14\%$  even at the core radius of  $0.1r_\star$ . Differencing two maps in orthogonal linear polarization is potentially a way to improve the signal-to-noise ratio. More importantly perhaps is that the presence of polarization would be a clear signal that the measured halo was a  $\text{Ly}\alpha$  halo of the type described here rather than some other, possibly instrumental, effect.

## 5. Conclusions

We have shown that  $\text{Ly}\alpha$  sources before the reionization redshift should be surrounded by an intergalactic halo of scattered  $\text{Ly}\alpha$  photons. These sources are expected to appear more spatially extended in the  $\text{Ly}\alpha$  line than they are in the continuum to the red of the line. Our numerical solution implies that the  $\text{Ly}\alpha$  halo has a roughly uniform surface brightness out to an impact parameter  $p \sim 0.1r_\star \approx 70 \text{ kpc}$  (see Fig. 1). At this impact parameter, the line is broadened and redshifted by of order  $\sim 10^3 \text{ km s}^{-1}$  relative to the source (Fig. 3). These substantial broadening and redshift signatures cannot be easily caused by galactic kinematics and hence signal the intergalactic origin of the scattered line.

The detection of intergalactic  $\text{Ly}\alpha$  halos with the above characteristics around sources down to a limiting redshift at which the neutral IGM ceases to exist, can be used as a direct method for inferring the redshift of reionization. Alternative methods are more ambiguous, as they rely on the detection the Gunn-Peterson damping wing which might be confused with damped  $\text{Ly}\alpha$  absorbers along the line-of-sight (Miralda-Escudé 1998; see also Haiman & Loeb 1999 for  $z_s \lesssim 7$ ), the detection of the weak damping factor of small-scale microwave anisotropies which is an integral quantity depending also on other cosmological parameters (e.g., Hu & White 1997; Haiman & Loeb 1998a), or the detection of very faint (and somewhat uncertain) spectral features in the cosmic background which is highly challenging technologically (Haiman, Rees, & Loeb 1997; Gnedin & Ostriker 1997; Baltz, Gnedin, & Silk 1998; Shaver et al. 1999).

Our calculation assumed the simplest configuration of a uniform, neutral, IGM with a pure Hubble flow around a steady Ly $\alpha$  source. In popular Cold Dark Matter cosmologies, the characteristic nonlinear mass scale of collapsed objects at  $z_s \gtrsim 10$  is  $\lesssim 10^8 M_\odot$  (e.g., Haiman & Loeb 1998a). A galaxy of total mass  $10^8 M_8 M_\odot$  is assembled from a radius of  $4.4(M_8/\Omega_M h_0^2)^{1/3}[(1+z_s)/10]^{-1}$  kpc in the IGM, which is more than an order of magnitude smaller than our inferred Ly $\alpha$  halo radius. Similarly, the Hubble velocity at the Ly $\alpha$  halo radius is larger by more than an order of magnitude than the characteristic velocity scale of nonlinear objects at these redshifts. Hence, our simplifying assumptions of a smooth IGM immersed in a Hubble flow are likely to be satisfied on the Ly $\alpha$  halo scale. Modest corrections due to the density enhancements and peculiar velocities in the infall regions around sources might, however, be necessary. More importantly, the ionization effect of a bright quasar on its surrounding IGM might extend out to the scale of interest. In such a case, the intensity distribution of the Ly $\alpha$  halo will depend on the spectrum and luminosity history of the ionizing radiation emitted by the source, which determine the neutral fraction as a function of radius around it. This “proximity effect” might be important for quasars but less so for galaxies whose ultraviolet emission is typically strongly suppressed beyond the Lyman limit due to absorption in stellar atmospheres and in the interstellar medium. Other changes to the halo intensity and polarization profiles might result from short-term variability (on  $\lesssim 10^5$  years) or anisotropic Ly $\alpha$  emission by the source. These complications could be easily incorporated into our Monte Carlo approach, for particular source parameters.

Detection of the predicted Ly $\alpha$  halo might become feasible over the next decade either with larger ground-based telescopes or with the Next Generation Space Telescope<sup>5</sup> (NGST). For  $z_s \sim 10$ , the entire Ly $\alpha$  luminosity of a source is typically scattered over a characteristic angular radius of  $\sim 15''$ . The Ly $\alpha$  halo is therefore sufficiently extended to be resolved along with its tangential polarization, as long as its brightness exceeds the fluctuation noise of the infrared background.

Recently, five sources have been photometrically identified to have possible redshifts of  $z \gtrsim 10$  in the Hubble Deep Field South observed by NICMOS (Chen et al. 1998). We emphasize that even just a narrow-band photometric detection of the scattered Ly $\alpha$  halos (see Fig. 1) around sources at different redshifts would provide invaluable information about the neutral IGM before and during the reionization epoch. On sufficiently large scales where the Hubble flow is smooth and the IGM is neutral, the Ly $\alpha$  brightness distribution can also be used to determine the values of the cosmological mass densities of baryons and matter through equations (8), (9) and the angular diameter distance relation. Thus, in addition to studying the development of reionization, such observations could constrain fundamental cosmological parameters in a redshift interval that was never probed before.

---

<sup>5</sup>NGST is the successor to the Hubble Space Telescope which is planned for launch over the next decade. For more details, see <http://ngst.gsfc.nasa.gov/>.

Scattering of resonance line radiation gives rise to polarization at a level depending on the atomic physics of the transition and on the geometry of the scattering events. Using an extension of the Monte Carlo technique used here, Rybicki & Loeb (1999) showed that most photons with the largest impact parameters suffer a nearly right-angle last scattering, and the degree of tangential polarization is large for such photons, of order tens of percent (asymptotically 60%). Measurement of this polarization could be used as an independent check on the model parameters, and might even provide a powerful way of identifying early objects.

We thank Chris Kochanek and Chuck Steidel for useful discussions. This work was supported in part by the NASA grants NAG5-7768 and NAG5-7039 (for AL).

## REFERENCES

- Abel, T., Norman, M., & Madau, P. 1998, ApJ, submitted, astro-ph/9812151
- Baltz, E. A., Gnedin, N. Y., & Silk, J. 1998, ApJ, 493, L1
- Barkana, R., & Loeb, A. 1999, ApJ, submitted, astro-ph/9901114
- Carlberg, R. G., et al. 1998, Presented at Royal Society Discussion Meeting, March 1998, “Large Scale Structure in the Universe”; see astro-ph/9805131
- Chen, H.-W., Fernandez-Soto, A., Lanzetta, K. M., Pascarella, S. M., Puetter, R. C., Yahata, N., & Yahil, A., 1998, astro-ph/9812339; see the web site <http://www.ess.sunysb.edu/astro/hdfs/home.html>
- Dey, A., Spinrad, H., Stern, D., Graham, J. R., & Chaffee, F. H. 1998, ApJ, 498, L93
- Edwards, D. 1972, MNRAS 159, 51
- Eisenstein, D. J. 1997, astro-ph/9709054
- Etorri, S., & Fabian, A. C. 1999, MNRAS, in press, astro-ph/9901304
- Gnedin, N. Y., & Ostriker, J. P. 1997, ApJ, 486, 581
- Gunn, J. E., & Peterson, B. A. 1965, ApJ, 142, 1633
- Haiman, Z., & Loeb, A. 1998a, ApJ, 503, 505
- . 1998b, to appear in Proc. of “After the Dark Ages: When Galaxies Were Young”, Oct. 12-14, 1998, College Park, Maryland; astro-ph/9811395
- . 1999, ApJ, in press, astro-ph/9807070
- Haiman, Z., Rees, M. J., & Loeb, A. 1997, ApJ, 476, 458
- Harrington, J. P. 1973, MNRAS, 162, 43
- Hauser, M.G. et al. 1998, ApJ, 508, 25
- Hu, E. M., Cowie, L. L., & McMahon, R. G. 1998, ApJ, 502, L99

- Hu, W., & White, M. 1997, *ApJ*, 479, 568
- Hummer, D.G., & Rybicki, G.B. 1971, *MNRAS*, 152, 1
- Loeb, A. 1997, in *Proc. of “Science with the Next Generation Space Telescope”*, eds. E. Smith & A. Koratkar, pp. 73-86; astro-ph/9704290
- Mihalas, D. 1978, *Stellar Atmospheres*, W.H. Freeman, San Francisco 419
- Mihalas, D., Kunasz, P. B., & Hummer, D. G. 1976, *ApJ*, 210, 419
- Miralda-Escudé, J. 1998, *ApJ*, 501, 15
- Miralda-Escudé, J., & Rees, M. 1998, *ApJ*, 497, 21
- Miralda-Escudé, J., Haehnelt, M., & Rees, M. 1998, *ApJ*, submitted, astro-ph/9812306
- Narayan, R., Loeb, A. & Kumar, P. 1994, *ApJ*, 431, 359
- Neufeld, D. A., & McKee, C. F. 1988, *ApJ*, 331, L87
- Padmanabhan, T. 1993, *Structure Formation in the Universe*, Cambridge University Press, Cambridge, p. 67
- Peebles, P. J. E. 1993, *Principles of Physical Cosmology*, Princeton University Press, Princeton
- Rybicki, G., & Loeb, A. 1999, *ApJL*, submitted
- Shaver, P. A., Windhorst, R. A., Madau, P., & de Bruyn, A. G. 1999, *A & A*, submitted, astro-ph/9901320
- Spinrad, H., Stern, D., Bunker, A., Dey, A., Lanzetta, K., Yahil, A., Pascarelle, S., & Fernandez-Soto, A. 1998, *AJ*, 116, 2617
- Turner, M. 1999, in *Proceedings of the Nobel Symposium, Particle Physics and the Universe; Enköping, Sweden, August 20-25, 1998*; astro-ph/9901109
- Weymann, R. J., Stern, D., Bunker, A., Spinrad, H., Chaffee, F., Thompson, R. I., & Storrie-Lombardi, L. J., 1998, *ApJ*, 505, L95



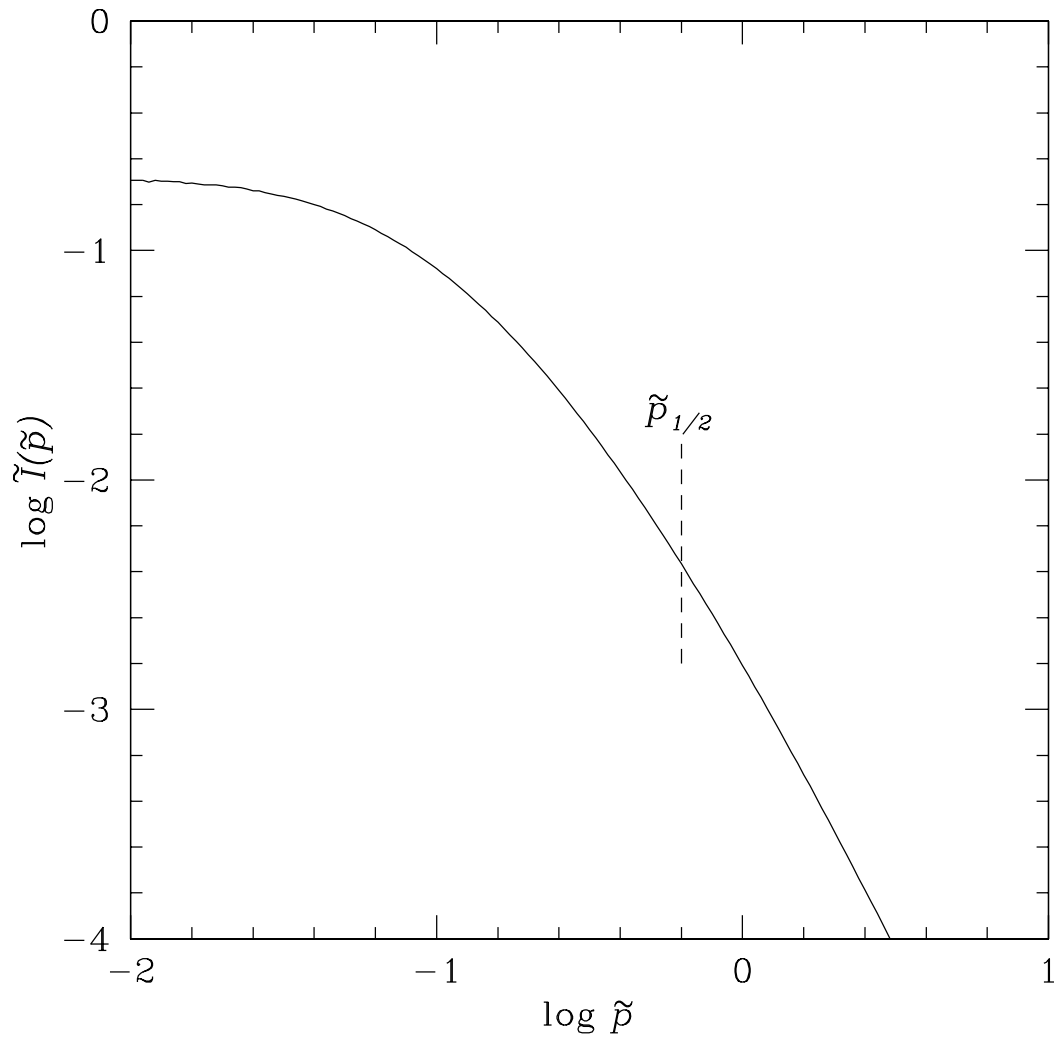


Fig. 1.— Integrated intensity,  $\tilde{I}(\tilde{p}) = \int_0^\infty \tilde{I} d\tilde{\nu}$ , versus impact parameter,  $\tilde{p}$ . The projected half light radius is denoted by  $\tilde{p}_{1/2}$ .

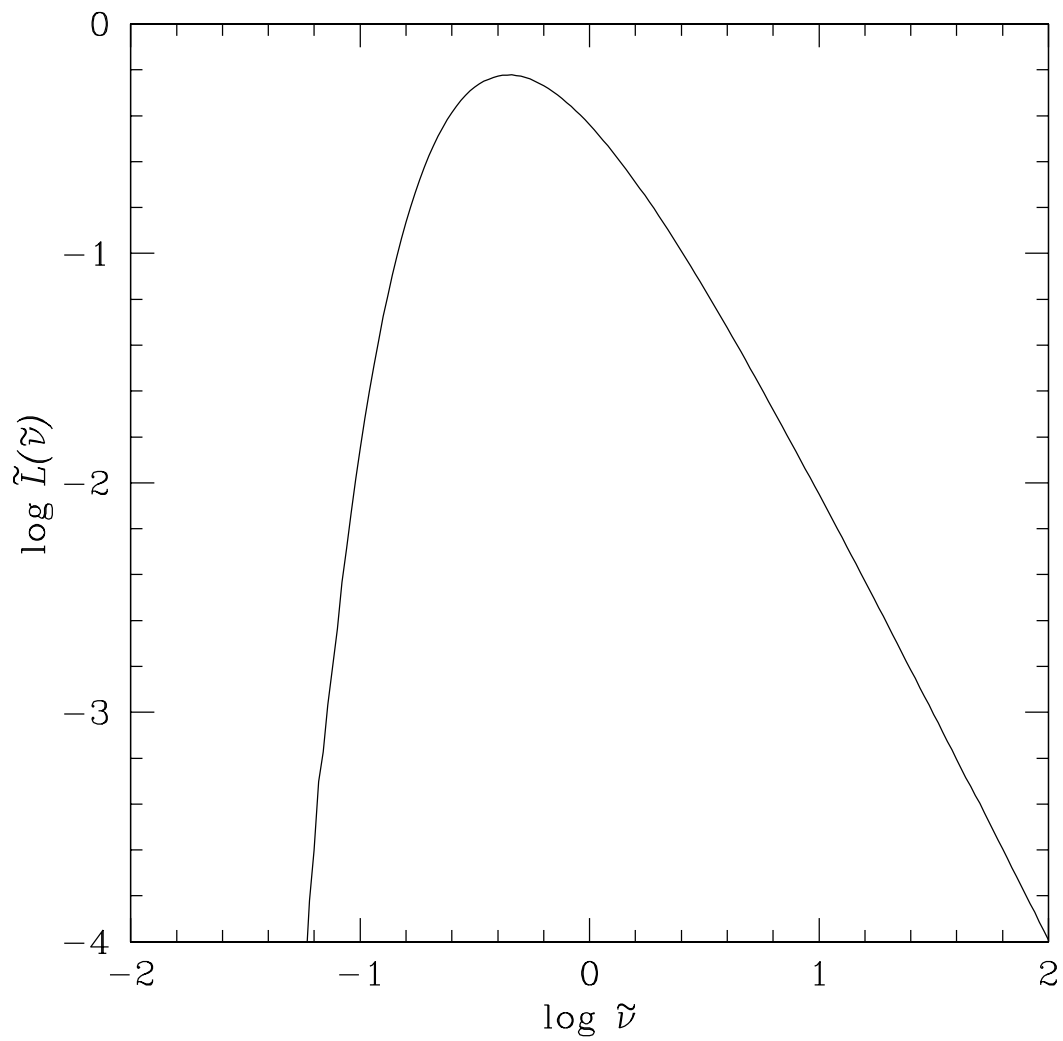


Fig. 2.— Monochromatic photon luminosity,  $\tilde{L}(\tilde{\nu}) = 8\pi^2 \int_0^\infty \tilde{I} \tilde{p} d\tilde{p}$ , as a function of frequency redshift,  $\tilde{\nu}$ .

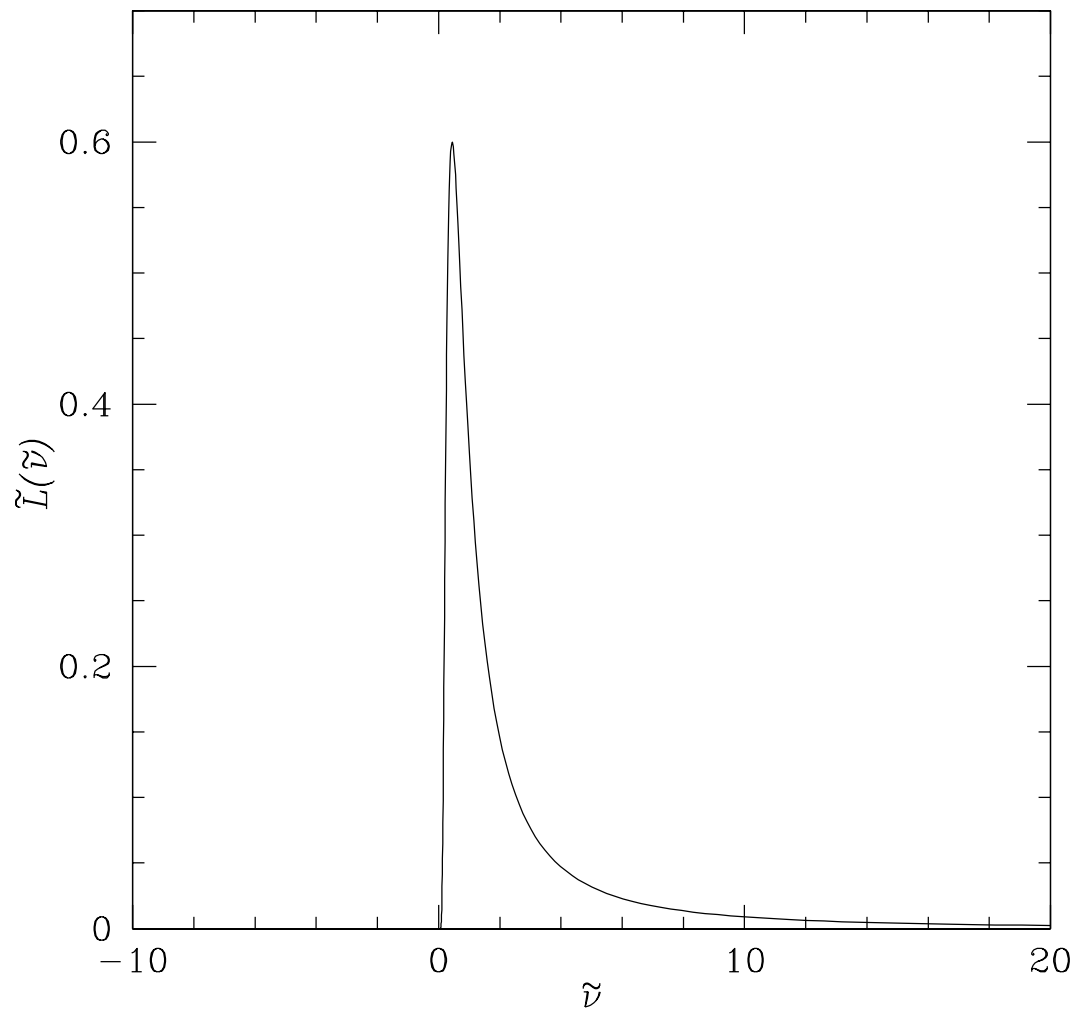


Fig. 3.— Same as Figure 2, but using linear scales.

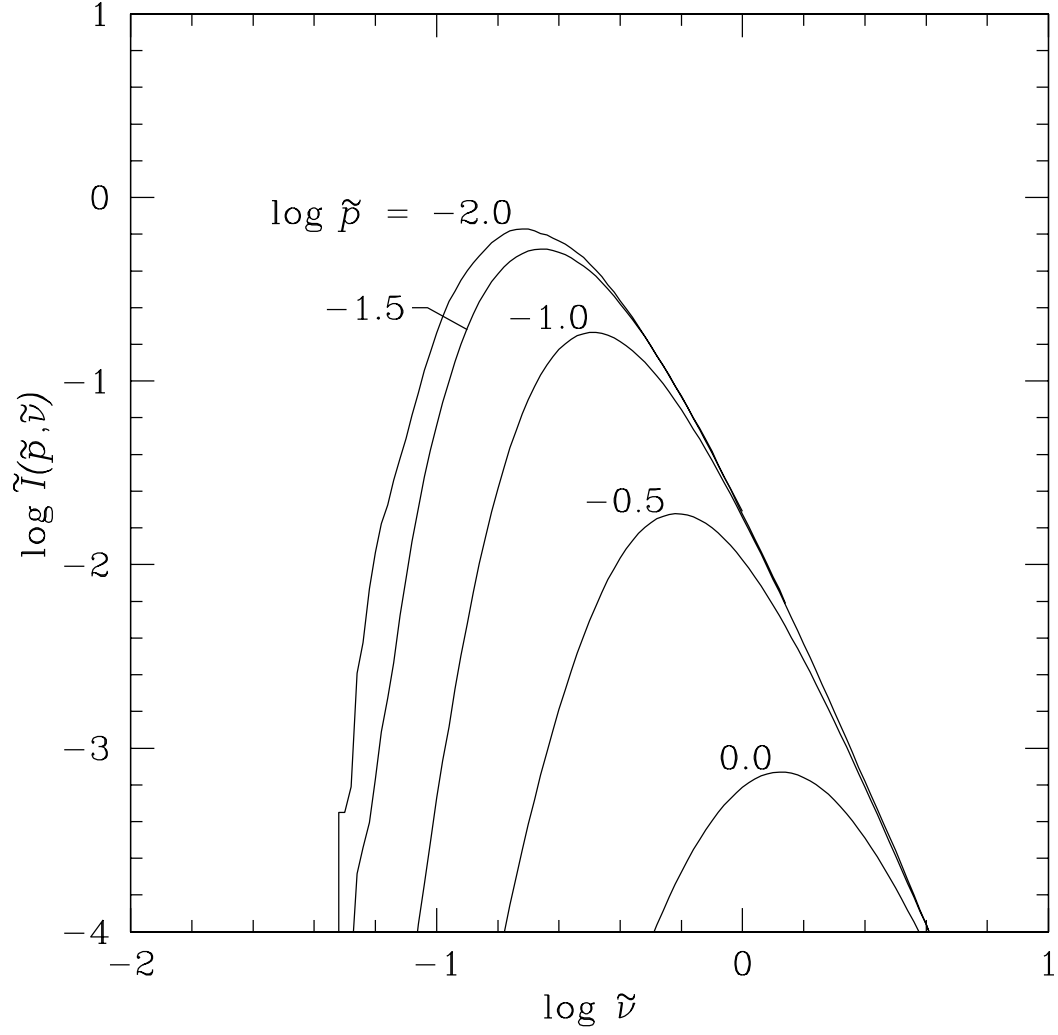


Fig. 4.— Ly $\alpha$  line profiles. Curves of intensity,  $\tilde{I}(\tilde{p}, \tilde{\nu})$ , versus frequency shift to the red of resonance,  $\tilde{\nu}$ , at different values of the impact parameter,  $\tilde{p}$ .

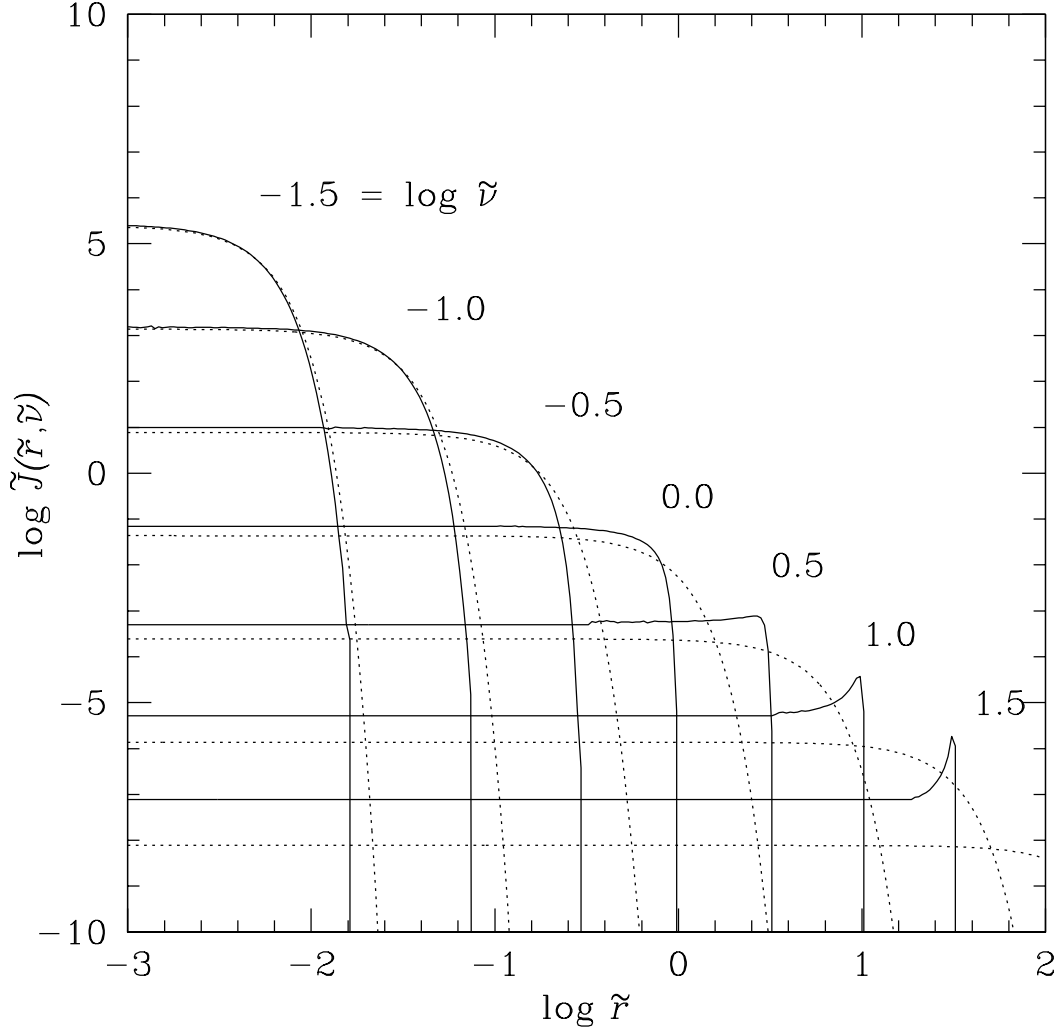


Fig. 5.— Curves of the monochromatic mean intensity,  $\tilde{J}(\tilde{r}, \tilde{\nu})$ , versus radius,  $\tilde{r}$ , at different values of the frequency redshift,  $\tilde{\nu}$ . Note that in agreement with the “causal” diffusion equation (18),  $\tilde{r} \leq f^{1/2}\tilde{\nu}$ , where  $f = 1/3$  in the diffusion regime ( $\tilde{r} \ll 1$ ) and  $f = 1$  in the free-streaming regime ( $\tilde{r} \gg 1$ ). The dotted lines show the analytic solution (21) for the diffusion regime.